SAND2010-7860C
11BFL-0002

Laser ignition of multi-injection gasoline sprays

Author, co-author (Do NOT enter this information. It will be pulled from participant tab in MyTechZone)

Affiliation (Do NOT enter this information. It will be pulled from participant tab in MyTechZone)

ABSTRACT

Laser plasma ignition has been pursued as an alternative to electric spark ignition systems, potentially offering benefits by avoiding quenching surfaces and extending breakdown limits at higher boost pressure and lower equivalence ratio. For this study, we demonstrate another potential benefit: the ability to control the timing of ignition with short, nanosecond pulses, thereby optimizing the type of mixture that burns in rapidly changing, stratified fuel-air mixtures. We study laser ignition at various timings during single and double injections at simulated gasoline engine conditions within a controlled, high-temperature, high-pressure vessel. Laser ignition is accomplished with a single low-energy (10 mJ), short duration (8 ns) Nd:YAG laser beam that is tightly focused (0.015 mm $1/e^2$ diameter) at a typical GDI spark plug location. Ignition timing is varied during, after, and between injections of a rapid, 0.4-ms/0.4-ms dwell/0.4-ms injection schedule. Results show success in igniting a single injection after the end of injection, but with poor combustion efficiency because the flame does not move downstream to earlier-injected charge. Findings are similar when igniting after the end of a double injection. Best results are observed when igniting between injections. The tail of the first injection ignites, and the second injection acts to pull the flame downstream to the first-injection charge, causing high combustion efficiency. However, the timing of ignition between pulses is critical. If ignited too soon after the end of the first injection, ignition may fail or, if ignition succeeds, the flame grows such that it immediately ignites the second injection, forming fuel-rich combustion and significant soot generation. The optimal timing produces no soot formation, but still maintains high combustion efficiency. However, accomplishment of this timing requires ignition timing control on the order of 0.1 ms, which is much shorter than current electric spark ignition systems that have spark durations on the order of 1.0 ms. Therefore, the benefits of this double-injection ignition strategy are only realized with the use of a short-pulse laser ignition system.

INTRODUCTION

Current electric spark-ignition systems present a limitation in the development of modern lean-burn spark-ignited direct-injection (SIDI) gasoline engines. To achieve high efficiency and low NO_x emissions, direct-injection gasoline engines are increasingly using high rates of exhaust gas residual, high boost pressures, and globally lean fuel-air ratios [1] – conditions where electric spark-ignition systems can display misfire and poor cycle-to-cycle combustion stability[2]. When used in spray-guided geometries, where the spray and spark electrodes are closely coupled, steep gradients of equivalence ratio and velocity are present at the spark gap, and mixtures can rapidly fall outside ignition stability ranges [3,4]. In addition, the presence of high velocities and turbulent fluctuations at the spark gap, in combination with long spark duration times (1-3 ms) can cause the spark channel to become highly stretched [4,5,7], potentially encompassing a wide range of equivalence ratios and velocity conditions. Thus, the initial ignition and kernel development can by highly asymmetric and subject to significant cycle-to-cycle fluctuations [8]. Indeed, the convective motion of the spark channel and initial kernel development play a key role in the tendency for misfire and it has been shown that convection of the kernel downward and away from the spark electrodes is critical for successful flame propagation through a stratified fuel jet [5,6]. The spark plug electrodes themselves can also influence initial kernel development, quenching early flame development, disrupting in-cylinder flows, and promoting asymmetric flame propagation [8,9]. Finally, the electrodes are also prone to spray wetting and fouling, and become a source of soot formation [3].

To improve the ignition and combustion stability of lean-burn SIDI engines, new methods of fuel delivery and ignition strategies have become of significant interest. The use of multiple fuel injections has become more prominent, leveraging the reduced momentum of short, small injections, to reduce spray penetration [7,10,11]. Thus, fuel-air mixtures are kept in closer proximity to the spark gap [10,11] and local flow velocities that can stretch and extinguish developing spark kernels are reduced [7]. Multiple-spark ignition

systems have also surfaced in the literature, employing up to 30 spark strikes per ignition cycle [2,7], which increases the probability of a successful ignition event [2] and limits the time available for spark channel stretching [7]. Recent work by Yun, et al. [12] has combined these concepts in a multi-injection, multi-ignition (MIMI) operating strategy capable of operating at very light load conditions, where misfire conditions normally prevent fuel-lean operation. However, as modern SIDI engines become further downsized and pushed to higher boost pressures with higher EGR dilution, the fundamental challenges inherent to the ignition of lean, high-pressure, highly-dilute mixtures remain.

Laser-spark ignition displays attributes that may improve ignition, kernel development and flame propagation over conventional electric spark systems. Unlike conventional spark ignition, the energy requirement for breakdown actually decreases with increased ambient pressure [13]. Decreased ignition delay times are observed for laser-induced sparks in comparison with conventional electric sparks [8,14]. Laser-ignition also produces overdriven flame speeds, demonstrated in quiescent homogenous laser-ignited mixtures to produce flames that can momentarily propagate up to 20 times faster than the laminar flame speed [13]. These accelerated combustion timescales have the potential to shorten combustion duration and minimize cycle-to-cycle combustion variations. Another significant benefit is that the laser spark location is adjustable, allowing one to optimize the ignition location by positioning the ignition kernel where ideal equivalence ratio and velocity conditions exist for robust kernel development and flame propagation. Elimination of the spark electrodes also removes a heat sink from the kernel development region, allowing full energy transfer from the plasma to the developing kernel. Laser spark has also been demonstrated to extend lean flammability limits [15].

Indeed, the use of laser-spark ignition has been successfully demonstrated in SIDI engines, with indications that laser-induced sparks improve some combustion characteristics compared to conventional sparks for homogeneous operation. Febler, et al. [8] and Groβ.,et al. [14] have directly compared laser-induced spark and electric spark in SIDI optically-accessible engines under homogeneous charge operation. Both groups found decreased ignition delay times and more rapid kernel growth when employing laser-induced spark. These characteristics led to improved combustion stability of the engine, as manifested by a lower coefficient of variation (COV) of IMEP [14]. Furthermore, chemiluminescence imaging of the developing kernels showed that in the absence of intruding electrodes, the laser-ignited flame propagation is nearly spherical, with less cyclic variability in propagation speed and flame front geometry [8]. Tsunekane, et al. [16] have also demonstrated successful ignition with extremely low laser-ignition energy, near 2 mJ, illustrating the potential for practical application.

The success of laser-ignition for SIDI engines under stratified charge operation is less straightforward. Febler, et al. [8] and Groβ, et al. [14] both found that when switching to spray-guided operation, the ignition delay and combustion stability for electric-spark and laser-spark ignition became more similar, though laser-induced sparks still displayed slightly faster ignition and flame growth. The similarity arose because the plasma location for both ignition systems was collocated with a fuel-rich portion of the spray, where ignition delays are short. In addition, sporadic misfire was observed for laser-ignition operation that was not observed with electric spark. These sporadic misfire events are not well understood, but likely arise from the temporal and spatial scales of laser-induced ignition relative to the turbulent stratified mixing of the fuel spray. While an electric-spark discharge can last up to2-3 ms [4,5,8], with the spark channel stretching up to 10 mm in a highly turbulent flow [4], a high-energy Q-switched laser pulse will last on the order of 10 ns and will be focused into a diameter that is on the order of a few micrometers to achieve breakdown. These condensed spatial and temporal scales, overlaid onto a highly turbulent stratified flow, are certain to contribute to an increasing probability that the velocity and equivalence ratio of the mixtures within the spark location will be outside of ignition limits.

Though the application of laser-spark ignition in stratified-charge SIDI engines has been met with some challenges due to condensed spatial and temporal timescales, it is precisely those characteristics that may help us better understand ignition and combustion processes under these operating conditions. For example, the application of multi-spark operating strategies with conventional electric spark systems does not enable a complete understanding of optimal timing windows and mixture conditions for ignition due to inherently long spark durations. For a spark-duration of 2 ms at an engine speed of 2000 rpm, the spark channel will persist for approximately 24 crank angle degrees (CAD). Local flow conditions are certain to vary widely over this period, confounding one's ability to understand the role of local mixture equivalence ratio, velocity or turbulence levels on ignition processes. In addition, there is potential for improved NO_x and soot emissions control with the ability to more precisely control spark timing, thereby offering more control over the mixture equivalence ratios that participate in the ignition and combustion process.

In the current study, we exploit the condensed time and spatial scales of laser ignition to more precisely define ignition windows for spray-guided ignition and gain an improved understanding of the optimal conditions for successful stratified combustion. In addition, we explore the laser ignition process in detail to develop an understanding of the plasma length and timescales under engine operating conditions. We also leverage the capability of our combustion vessel facility to provide direct visualization of the flame propagation over a large field of view, beyond that achievable in a typical optically-accessible engine, and without the confounding influence of piston motion and in-cylinder flows. In summary, we seek to provide a more fundamental picture of laser-induced ignition in sprays, while simultaneously exploring the potential for precision ignition of multiple injection sprays.

EXPERIMENTAL SETUP

COMBUSTION VESSEL AND LASER IGNITION SETUP

Experiments were performed in a constant-volume combustion vessel under simulated, quiescent, engine conditions. A schematic of the combustion vessel is illustrated in Figure 1. The combustion chamber is cubical, measuring 108 mm on each side. As shown in Figure 1, a Bosch automotive GDI fuel injector is mounted in one of the four side-ports. Three sides of the cubical combustion chamber are fitted with 100-mm-diameter sapphire windows (2 side ports and the bottom-access port) and one side port is fitted with an aspheric lens-window for access and focusing of the laser-ignition beam. These optically-accessible ports provide a large field-of-view and permit several viewing angles of the injected fuel spray. The remaining side-port at the top of the vessel is installed with two spark plugs for initiating the premixed combustion event, which generates high-temperature and high-pressure ambient conditions inside the vessel, as described below.

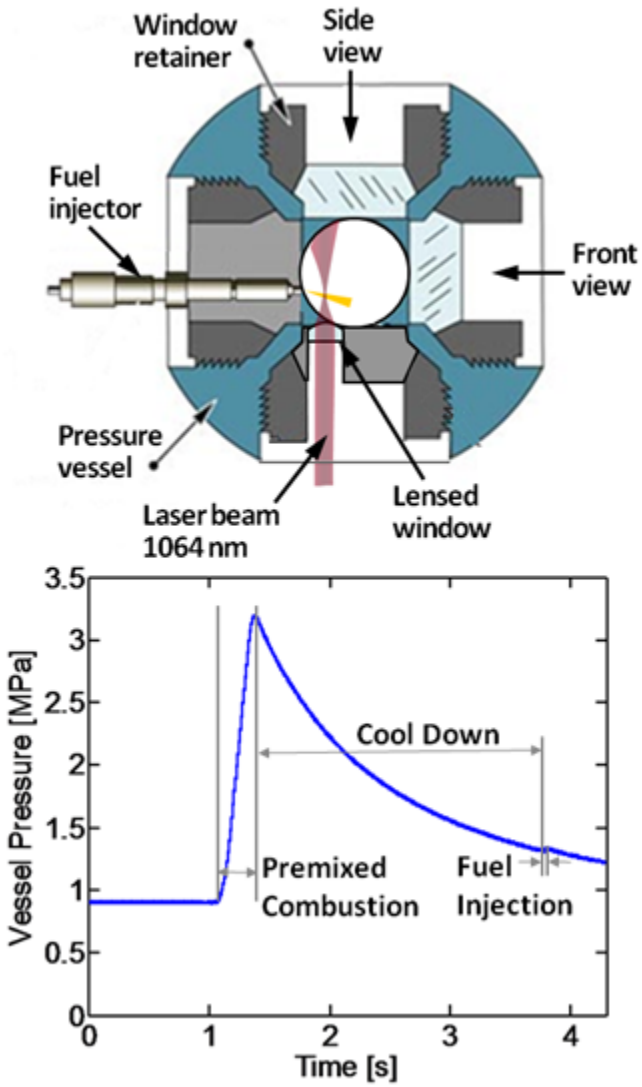

Figure 1: Top-view schematic of constant-volume combustion vessel (above) and example of pre-burn operating procedure to create high-pressure and high-temperature ambient environments (below).

Engine conditions are simulated by using a premixed, combustible-gases mixture, which is spark-ignited to create a high-temperature, high-pressure environment in the vessel. Following the premixed combustion, the combustion products cool over a relatively long time (~1-3 s) due to heat transfer to the vessel walls and the vessel pressure slowly decreases. A typical measurement of the vessel pressure is shown at the bottom of Figure 1. When the desired pressure and temperature is reached, the fuel injector is triggered and

fuel injection occurs. A mixing fan is used to maintain the uniformity of the ambient gases within the vessel. Particle tracking velocimetry shows random velocities less than 0.1 m/s exist within the chamber, making the ambient gases essentially quiescent. A detailed description of this facility and its operation can be found in [17].

The temperature, density, and composition of the ambient gas in the vessel at the time of fuel injection can be varied widely with this simulation procedure. The conditions of the ambient gas at the start of injection are determined by the initial mass and composition of gas within the vessel and the pressure at the time of fuel injection. All experiments were performed in an environment of 21% O_2, simulating undiluted combustion in air (i.e. no exhaust gas recirculation). Table 1 shows the ambient gas condition that was employed in this study. The ambient gas pressure and density are representative of in-cylinder conditions for an automotive engine with a 12:1 compression ratio, an intake pressure of 1 bar absolute, and a spark timing of 30° before top-dead-center (BTDC). Temperature measurements in the vessel were performed by fine-wire thermometry to establish a relationship between pressure and the temperature during the cool down. The gas temperature was uniform to within 1% along the axial direction [18].

The fuel injector specifications and operating conditions are outlined at the bottom of Table 1. Iso-octane fuel was delivered through the Bosch GDI injector at 100 bar. The fuel injector was equipped with a dual-spray nozzle, with the holes oriented at a 60° included angle with the injector axis. The holes are designed to provide the spray pattern of two adjacent sprays from a standard 8-hole GDI injector (i.e., 45° spacing between jets).

Laser ignition of the fuel spray was achieved by focusing a 1064-nm beam from a dual-head Nd:YAG laser, through a custom-designed fused-silica aspheric lens-window with a 30-mm focal distance. Prior to the focusing lens, the beam was approximately 3 mm in diameter. Only one of laser heads was used, providing a pulse energy of 10 mJ, with a pulse duration of 8 ns. The aspheric lens-window was fixed in a pressure-sealed translational mount so that the focal point of the beam could be located precisely in the fuel spray. For the experiments presented here, the focal point and fuel spray were oriented to provide an ignition location at the centerline of one of the two sprays, 15 mm downstream of the nozzle. Ignition locations between sprays were also investigated, but ignition was not found to be more stable than the spray-centerline position.

Table 1: Combustion vessel ambient gas conditions and fuel injector specifications

Ambient Conditions:	
Ambient gas temperature	700 K
Ambient gas pressure	1.3 MPa
Ambient gas density	6.5 kg/m^3
Ambient gas oxygen (by volume)	21% O2
Fuel Injector and Operating Conditions:	
Fuel injector (2-hole)	Bosch GDI solenoid-activated
Hole spacing	45°
Spray full included angle	60°
Fuel injection pressure	100 bar
Fuel	Iso-octane
Fuel temperature at nozzle	363 K (90°C)
Single injection duration	1.2 ms
Single injection mass	~2.7 mg
Double injection schedule	0.4/0.35 dwell/0.4 ms
Double injection mass	~1.8 mg

DIAGNOSTICS

High-speed imaging systems tracked the liquid and vapor phase development of the sprays, similar to Ref. [19]. Both of these measurements were performed prior to the installation of the laser-ignition focusing lens, with a 100-mm-diameter sapphire window installed in its place. By tracking the transient development of the liquid and vapor-phase fuel in the spray, we identify the temporal and spatial location of the laser-ignition point relative to important spray development events. After installing the laser-ignition focusing lens, we utilized the high-speed imaging system to record natural luminosity from chemiluminescence and soot. These

measurements provided detailed imaging of the laser-generated plasma, early kernel development and subsequent flame propagation in the spray.

Liquid-Phase Spray Imaging

Scattered light from fuel spray liquid droplets was imaged using a high-speed CMOS camera and a frequency-doubled, continuous-wave Nd:YAG laser operating with 2.5 W at 532 nm. The laser was formed into a volume and passed at a slight angle over the spray to illuminate only the liquid-phase region of the spray and to avoid interference with the simultaneous schlieren measurement (discussed below). A volume-illumination method, rather than a laser sheet, was utilized to ensure that all droplets spreading from the nozzle were illuminated, enabling identification of the maximum axial and radial distances of any liquid-phase fuel [20].

A high-speed CMOS camera, fitted with a 50-mm focal length f/1.2 lens, was used to image Mie-scattered light at a near-right angle to the path of the laser beam from the bottom access-port in the combustion vessel. The camera was operated at reduced resolution (256 x 128 pixels), allowing for fast framing periods (~21 μs) needed to capture dynamics of the developing fuel sprays. The lens was set to the maximum aperture (f/1.2) and the camera at an exposure duration (19 μs) to intentionally saturate the camera in the dense region of the spray while leaving sufficient dynamic range to identify regions of the spray where liquid completely evaporates.

Vapor-Phase Jet Imaging

A schlieren system was operated simultaneously with the Mie-scatter system described above using a second high-speed CMOS camera. A 150-W (electrical power) mercury-xenon arc lamp with a small (1.7-mm) arc distance was used as a white light source. Light from the arc was spatially-filtered through a 1-mm aperture and collimated to pass through two of the optically-accessible side ports in the combustion vessel, or through the side-view labeled in Figure 1. The collimated beam was then re-focused onto a high-speed CMOS camera equipped with a Nikkor lens and a 532-nm 0°-incidence laser mirror, which acted to block Mie-scattered light from spray droplets. The camera was operated at a resolution of 256 x 128 pixels, allowing for framing periods of approximately 21 μs. The exposure duration was 2 μs.

Ignition and Flame Propagation

With the laser-ignition focusing lens in place, the laser plasma formation, flame kernel development and flame propagation were imaged with a pair of high-speed CMOS cameras. Both cameras used KG3 glass filters to block scatter from the 1064-nm ignition-source beam while permitting maximum collection at visible wavelengths. Broadband plasma emission, chemiluminescence, and soot luminosity are collected with this setup.

The first camera was left in the bottom-view position as that used for Mie-scatter detection, retaining the 50-mm focal length f/1.2 lens. This camera was operated at a resolution of 256 x 256 pixels, with a framing period of 38 μs and an exposure duration of 34 μs.

A second high-speed camera, fitted with a 105-mm focal length f/2.8 lens, simultaneously acquired images through the front-view of the chamber to give a second perspective on plasma and flame development. In particular, the plasma formation was imaged with greater temporal resolution and higher magnification. Since the duration of the plasma formation happens on shorter timescales, the camera was operated at a reduced resolution of 128 x 64 pixels, enabling framing periods of about 10 μs, with an exposure duration of 4 μs. Stages of the laser-generated plasma were also measured without the presence of the spray. For these experiments, the combustion vessel was filled with nitrogen to 0.8 MPa, producing an ambient density of 6.5 kg/m^3 – equivalent to that of the laser-ignition operating condition outlined in Table 1.

In addition to high-speed luminosity imaging, a photodiode was simultaneously used to detect the spatially integrated chemiluminescence and soot luminosity from the reacting fuel jet. The photodiode was positioned to view the entire volume of the combustion chamber from the bottom.

The measured pressure within the chamber was also analyzed to determine ignition timing and the overall heat release from laser-ignited combustion. For this analysis, the pressure decay during the vessel cool down was removed (subtracted) to yield the pressure rise caused only by combustion [17].

RESULTS AND DISCUSSION

In the first section of results, we present high-speed imaging of the fuel spray development under non-igniting conditions. These images provide an understanding of the temporal and spatial scales of the fuel injection process. In the second section, we present high-speed imaging of the laser-induced plasma formation in a high-pressure nitrogen environment. By operating without the fuel spray, we can better understand plasma formation under these pressures without the confounding effects of chemical reaction. These two sections provide a foundational understanding of the temporal and spatial scales of these events, enabling a more complete interpretation of the laser-ignited spray results. The last two sections present laser-induced ignition of single and multiple-injection fuel sprays. In these sections, we explore the influence of ignition timing on kernel development and combustion by exploiting the precision timing capabilities of laser-induced ignition.

SPRAY CHARACTERIZATION

Figure 2 presents high-speed schlieren and Mie-scatter imaging of the fuel injection process. The injector nozzle is mounted in a conical metal port (the dark curved surface at the left of the schlieren images), with the tip of the injector protruding about 1 mm beyond the mount. In the schlieren images on the left side of Figure 2, the sprays are oriented in the mount such that they penetrate at equal angles above and below the injector nozzle axis (labeled as 0 mm on the left axis). Since the nozzle holes are oriented to produce a 60° full included angle, the sprays also penetrate at a 30° angle into the horizontal plane of the image. This 30° angle is apparent in the Mie-scatter images on the right side of Figure 2, where the sprays are imaged from below. From below, both sprays lie in the same vertical plane so that the scattered light appears to originate from a single penetrating spray. Note that because the sprays penetrate at a 30° angle into the schlieren image plane, the actual penetration distances are longer than derived from the horizontal scale at the bottom of the images. The timings shown at the bottom-right corner of each image are relative to the time after end of injection (AEI). The fuel injection begins at approximately -1200 μs.

The schlieren images identify refractive index gradients in the vaporizing spray that diffract the collimated light source. [21]. This technique enables visualization of the vaporized fuel boundary from the background ambient gases. Furthermore, high-density fluids have a higher index of refraction and cause greater beam steering. Thus, darker regions of the images indicate regions of denser mixtures. Liquid-phase fuel in the spray further causes significant darkening of the image due to extinction of light by scattering. The extent of liquid phase fuel in the spray is verified by simultaneous Mie-scatter imaging, shown on the right side of Figure 2.

Near the start of injection, during the first 10 mm of horizontal penetration, the two individual sprays appear distinct and dark against the background in the schlieren images. The subtle flow structures that appear in the background are due to boundary layers that form at the optical windows. The darkness of the sprays indicates that they are likely to be mostly liquid at this point, which is confirmed by the Mie-scatter images showing about 10 mm of horizontal penetration in the first image frame. As the sprays penetrate further downstream, mixing with hot ambient gases, vapor structures appear at the head of the two fuel jets. By about 900 μs after the start of injection (-298 μs AEI), the two sprays appear merged into one fuel jet with liquid-phase fuel extending from the nozzle holes to about 30 mm downstream. After the end of injection, these high-density liquid regions are mixed out rapidly – between 200 and 600 μs AEI, all of the initially dark regions are gone and the Mie-scatter images show nearly complete vaporization of the liquid fuel by 522 μs.

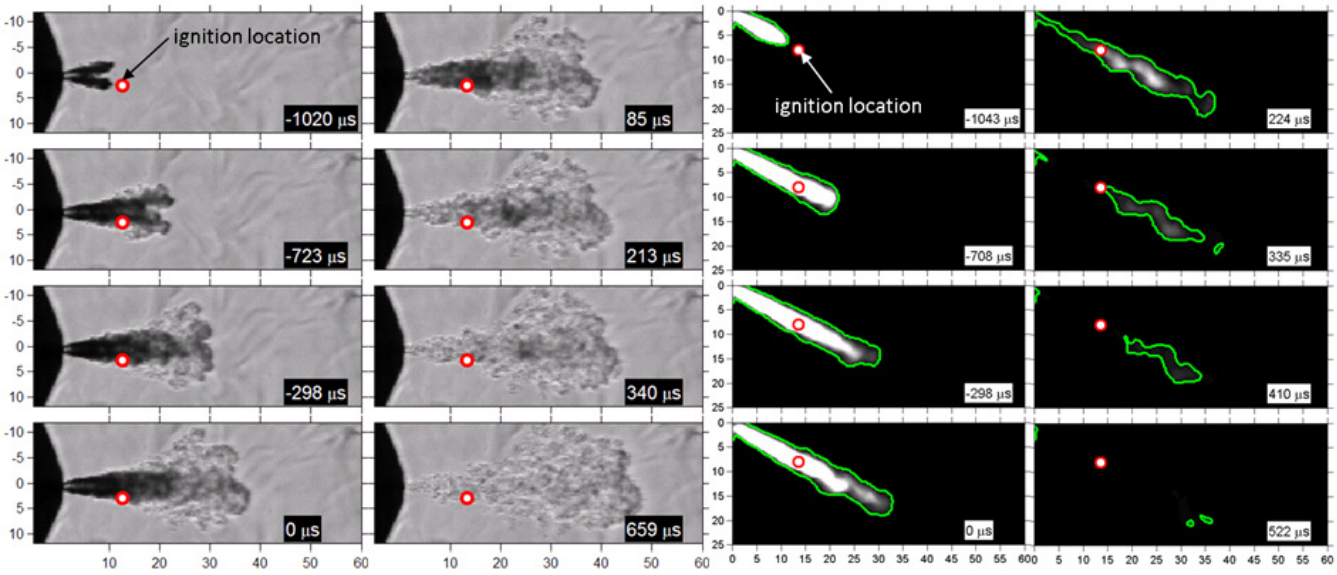

Figure 2: Schlieren (left) and Mie-scatter (right) imaging of spray development before and after end-of-injection. Axes shown at the bottom and sides of the images indicate distance in mm from injector nozzle tip. The green boundary surrounding the liquid Mie-scatter imaging indicates a threshold of 200 counts (out of 4096 counts).

As illustrated in Figure 2, the laser-ignition source beam was focused at the centerline of the lower fuel spray, 15 mm downstream of the injector nozzle in the direction of the spray (13.5 mm axial distance). A range of ignition timings were applied in this work before and after the end of injection, from approximately -600 µs AEI to 600 µs AEI. During injection, at approximately -600 µs AEI, Figure 2 shows that the focal point is situated in a region that is likely comprised of a dense cloud of liquid droplets. By about 200-300 µs AEI, schlieren images show that mixtures at the focal point transition from some darker high-density mixtures, where liquid is seen in the Mie-scatter images, to mixtures that are more uniform in refractive index gradients. Later, at 659 µs AEI, shortly after the time of the latest ignition timing of 600 µs, the refractive index of the mixtures in the ignition location of the fuel jet begins to match the background, indicating that fuel-air mixtures are at a density close to that of the background—mixtures are likely fuel lean and at high temperature [22]. The Mie-scatter images reflect the rapid transition in mixing after the end of injection. The scattered intensity weakens significantly, particularly in the region just downstream in the injector. The Mie-scatter images indicate that little to no liquid fuel exists at the ignition location shortly after 330 µs.

The observed changes in liquid vaporization and mixing that occur after the end of injection are consistent with previous observations in engine sprays. Studies show enhanced entrainment of the ambient gases occurs during the ramp down of injection rate near the end of injection [22-23]. The enhanced entrainment begins at the injector and propagates downstream with increasing time AEI producing mixtures that are progressively more fuel-lean towards the injector [22]. The additional entrainment of hot ambient gases serves to vaporize liquid fuel [23]. Although the more fuel-rich mixtures are eventually found downstream after the end of injection, not all fuel moves downstream. The schlieren images show substantial fuel vapor remains near the injector whilst liquid (and fuel-rich mixtures) progress downstream. As will be shown, successful combustion is highly dependent upon the ignition timing in this time-varying mixture.

LASER-GENERATED PLASMA FORMATION

Due to the transient nature of the spray development and vaporization process discussed above, it is apparent that the successful ignition of these highly stratified transient mixtures is likely to be sensitive to the characteristics of the laser-ignition source. Mixture gradients are expected to be high, both temporally and spatially, which means that the temporal and spatial characteristics of the ignition source will be of high importance. Thus, successful ignition will depend on not only the input energy, but also on how that energy is directed into the mixture. Characteristics such as the size of the focal volume, the energy density distribution produced at the focal point, and the time period that the deposited energy influences the surrounding mixtures, will all contribute to the success or lack of success in producing ignition. In the end, successful ignition will depend on the interaction of these characteristics with the temporally and spatially stratified flow. In the previous section, we discussed the temporal and spatial behavior of the fuel sprays that we are igniting. In this section, we discuss the temporal and spatial behavior of the laser-ignition beam and the resulting laser generated plasma.

Figure 3 presents the measured beam intensity distribution at the focus and estimated depth of focus for the input beam used in the laser-ignition experiments. Fitting to a Gaussian, the focused beam has a $1/e^2$ diameters of 21 μm and 12 μm along the a- and b-axes indicated in Figure 1. Although the focus is not uniform in the a- and b- directions, either waist diameter d_w is much smaller than the depth of focus along the laser beam direction. The depth of focus *dof* is given by:

$$dof = \frac{\pi d_{w,meas}^2}{2\lambda M^2} \qquad (1)$$

where M^2 is the beam quality factor and λ is the laser wavelength. An upper bound for *dof* is found assuming a Gaussian beam (M^2 = 1) and using the larger waist diameter, yielding *dof* = 650 μm. This estimate is clearly an upper bound as deviation from a Gaussian beam will increase M^2 and decrease *dof*. Nevertheless, *dof* remains much longer than d_w for typical M^2 values. Therefore, the laser ignition probe volume is dominated by the depth-of-focus direction.

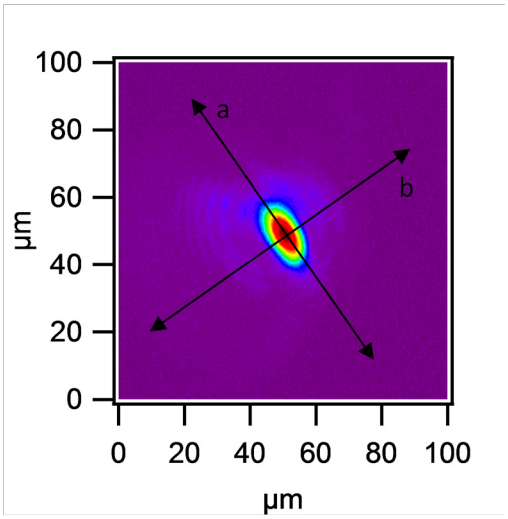

Figure 3: Focusing characteristics of the1064-nm laser-ignition beam.

Laser-induced ignition is based on generating electrical breakdown of gases into a high-energy high-temperature plasma, and we observe repeatable breakdown with a 10 mJ laser pulse energy with the beam-lens setup described above at the operating condition used in these experiments (Table 1). Based on the measured beam waist above, the estimated area-averaged power at the focal point is approximately $1x10^{12}$ W/mm^2 for a pulse energy of 10 mJ. In the presence of fuel vapor, the plasma breakdown threshold is reduced by the presence of fuel radicals. Indeed, we observe plasma formation in the presence of fuel at pulse energies as low as 2 mJ, with a formation probability of around 50%. By contrast, gas breakdown and plasma formation never occur for energies lower than 10 mJ in pressurized nitrogen environments at the same ambient density (with no fuel present).

To better understand the time scales of the breakdown and plasma formation process, we performed high speed imaging of the plasma luminosity. These images also provided a visual confirmation of the focal location relative to the spray geometry. The example shown in Figure 4is for an inert, nitrogen environment at 6.5 kg/m^3, which isolates the plasma behavior apart from the flame kernel development. When reaction occurs, it becomes difficult to separate the plasma lifetime from the flame kernel growth. Because of the increased difficulty in forming a plasma without fuel, as discussed above, 15-mJ laser energy is used in the example given in Figure 4.

The high-speed plasma imaging shown is conducted orthogonal to the laser beam propagation direction (the front view given in Figure 1). A schematic illustrating the relative location of the focusing lens, injector tip, and plasma imaging area are shown at the top of Figure 4 for reference. The laser-induced gas breakdown and plasma formation process begins with multiphoton ionization of the gases. The released electrons are accelerated by the absorption of additional photons, enabling the highly energetic electrons to further ionize the surrounding gas molecules. This electron cascade leads to electrical breakdown of the gases [13]. Note that this process is enhanced at high pressures due to increased collision frequencies. The first image in the plasma imaging sequence is shown at 21 μs after the arrival of the laser pulse. Prior to this time, the image is entirely saturated by luminosity produced during the high-energy gas breakdown. Following the time sequence through 41 μs after the arrival of the laser pulse, the plasma begins to develop a protruding

structure in the direction of the incident laser beam, referred to as the "third lobe" [13]. This structure is produced by gasdynamic effects following the shock and rarefraction waves that emanate from the plasma.

By 62 μs after the laser pulse, the plasma energy decays, contracting into a vertical oblong shape. Note that this vertical oblong shape is opposite the laser probe volume shape, but it occurs long after the laser timing. The plasma continues to decay and luminosity from the plasma is no longer visible after 62 μs. The images in Figure 4 indicate that the initial high energy plasma may extend to a region of about 2 mm in diameter, followed by energy decay over approximately 60 μs. Note that this plasma size is much larger than the waist and depth-of-focus dimensions discussed above, which may have important implications for successful ignition of spatially varying fuel-air mixtures. Although plasma imaging is shown here in a nitrogen environment, the plasma shape and lifetime does not change substantially when fuel is present. Thus, as a first criteria for laser-induced ignition, the chemical induction times for mixtures at the laser focal point must be on this timescale for successful ignition.

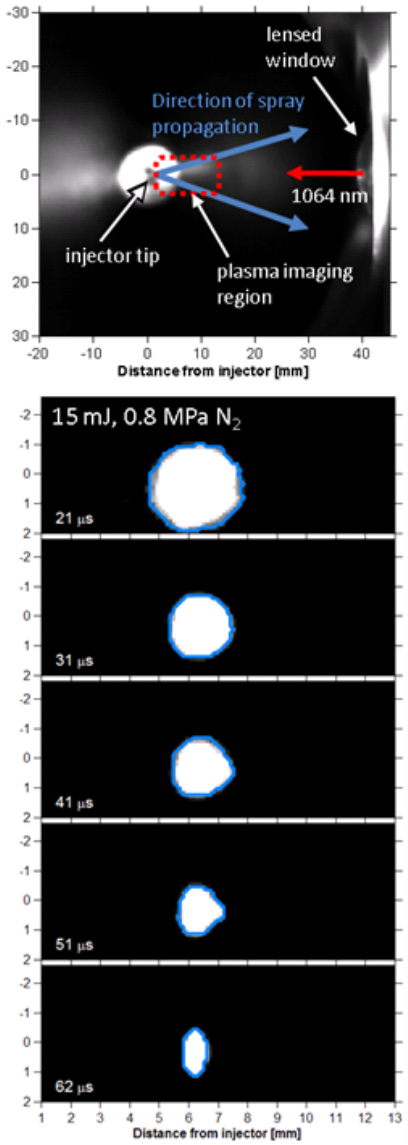

Figure 4: High-speed imaging of laser-induced plasma formation in nitrogen at 0.8 MPa The top image provides a schematic illustrating the location of the plasma imaging area relative to the injector nozzle and focusing lens.

INFLUENCE OF IGNITION TIMING ON KERNEL DEVELOPMENT AND FLAME PROPAGATION

Before characterizing laser ignition with multiple injections, we begin with single-injection events to determine the optimal timing of the laser relative to injection and to characterize the flame kernel development and propagation at these conditions. With the focal spot at an axial distance 14 mm from the injector, centered on the axis of the lower spray, the best laser timings for ignition occur after the end of injection, as will be shown below.

Figure 5 shows example luminosity images from the bottom view with the laser pulse arriving 340 μs AEI. Because of the significance of ignition timing relative to the end of injection, we will give timings relative to the end of first injection (AEFI) or second injection (AESI). The first luminosity images shown are prior to laser ignition, and before the time of complete evaporation of liquid droplets. As was shown in Figure 2, droplets mix and evaporate within several hundred microseconds AEFI. To aid visualization of this evaporation process, the liquid boundary of the spray is shown with a light green line in Figure 5. This boundary was identified by Mie-scatter imaging for separate injection events like that given in Figure 2, and is shown here at the same time AEFI. Likewise, the axial distance of the vapor boundary, identified by schlieren imaging (Figure 2), is shown as a dashed white line in the figure.

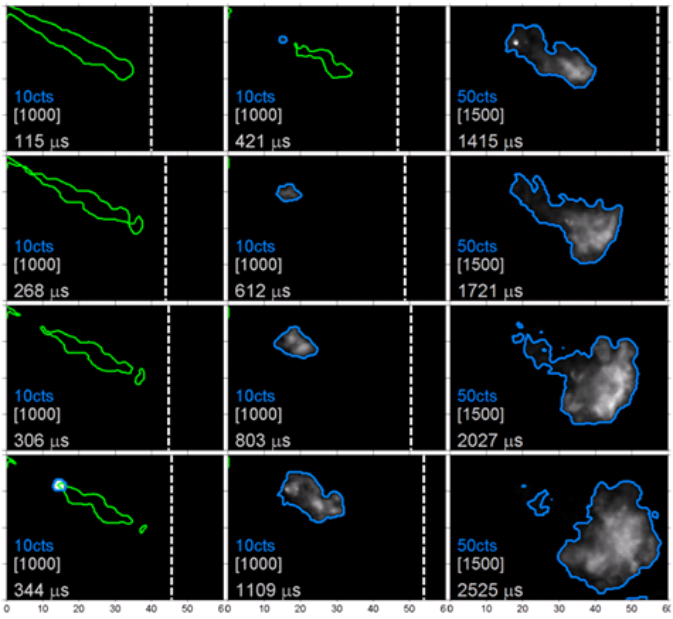

Figure 5: Laser ignition at 340 μs after end of 1200-μs duration single injection. Injector origin is upper left corner. Green: liquid boundary. White dashed line: axial vapor boundary. Blue: luminosity threshold at counts indicated. Brackets: grayscale counts display range.

Liquid droplets are beginning to move downstream of the ignition location at 300 μs AEFI, indicating that mainly a vaporized fuel-ambient mixture exists at the time of laser ignition. However, some droplets remain downstream. When the laser plasma becomes visible at 340 μs AEFI, the vaporized fuel charge has penetrated an axial distance from the injector of approximately 45 mm. Therefore, ignition upstream at 14 mm from the injector must form a flame kernel that will propagate downstream in order to consume most of the fuel charge.

The laser plasma appears bright at first, but the luminosity weakens and reveals only a small flame kernel by 420 μs AEFI. Afterwards, the flame grows in size and strengthens in intensity. To display both high and weak luminosities, we show the flame kernel development period and the main combustion period with different grayscale ranges in Figure 5. The maximum image count level of the display range is indicated in brackets on each image. We also show the boundary of the luminosity as a blue line corresponding to the threshold count levels indicated on each image. This convention will be followed in later figures.

The image sequence shows that the flame moves downstream towards the convective direction of the fuel spray, but it does not catch up to the axial vapor boundary (now past 60 mm) by 2500 μs AEFI. Significant fuel remains unburned at this time, but the flame

continues to propagate downstream after 2500 μs AEFI, eventually reaching the fuel vapor boundary determined by schlieren imaging. In contrast, the flame does not move substantially upstream of the ignition site during any time AEFI, which is most likely caused by several phenomena. First, flame speeds would need to exceed the convective flow velocity to make upstream progress towards the injector. Therefore, the most natural direction is to move downstream. Second, studies show that enhanced entrainment of the ambient gases occurs after the end of injection [22]. The enhanced entrainment begins at the injector and propagates downstream with increasing time AEFI, which quickly causes mixtures to become fuel-lean near the injector [22]. As such, there is too little fuel and mixtures are too fuel-lean to support flame propagation back to the injector [25]. Another observation from Figure 5 is that the flame intensity weakens in upstream regions that were once bright after ignition. This is partly because combustion is complete and the combustion products no longer have strong chemiluminescence from active radical pools. In addition, the reduced flame intensity results from enhanced upstream entrainment of ambient gases that dilutes the reacting mixture, potentially quenching some combustion regions, particularly those that are fuel-lean.

If the laser timing is advanced closer to the end of injection, ignition is not successful. A representative example is shown in Figure 6, which is for a laser timing of 70 μs AEFI. The sequence begins immediately AEFI when liquid droplets are present at the focal spot. Note that the weaker luminosity detected at the focal spot preceding the laser plasma is caused by flashlamp light from the laser that is scattered by the liquid droplets within the spray. Broadband plasma emission also illuminates the spray at 70 μs AEFI, saturating the camera at the focal spot and revealing upstream droplets extending back towards the injector. Although the plasma emission is very intense, no flame kernel develops afterwards. This laser ignition attempt is a complete misfire.

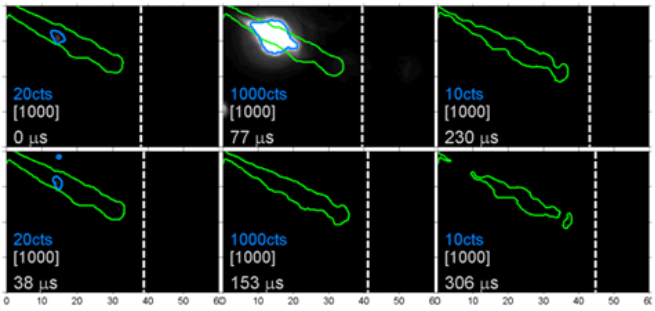

Figure 6: Laser ignition at 70 μs after end of 1200-μs duration single injection. Format the same as Fig. 5.

Summarizing the experiments with different laser timing, Figure 7 shows the timings AEFI corresponding to misfires and successful ignition at this focal spot position. For laser timings during injection until approximately 250 μs AEFI, ignition is not successful. Typical results are similar to that shown in Figure 6: the plasma immediately extinguishes and no flame kernel is formed. Failure to ignite most likely results from these mixtures being too fuel-rich to support flames, coupled with the fact that there are high scalar and velocity gradients that are also unfavorable to flame growth.

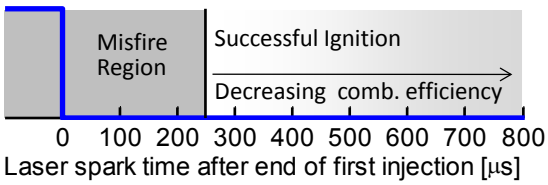

Figure 7: Schematic of successful ignition window for laser-induced ignition of a single fuel injection event ending at 0 μs. Injection schedule is indicated by the blue line. Dark regions indicate poor combustion as discussed in the text.

Ignition is successful when the mixture becomes more fuel-lean after the end of injection and droplets vaporize. However, delaying laser timing long AEFI results in flame kernels that do not grow quickly and, based on observations of pressure rise, the overall combustion efficiency decreases. The reduced combustion efficiency is shown as a grayscale intensity gradient in Figure 7. As alluded to above, the reasons for this decreased combustion efficiency are: (1) the main fuel charge continues to penetrate away from the ignition site with increasing time AEFI; (2) the mixture quickly becomes fuel-lean at the ignition location, making it less likely to support a flame; and (3) the convective velocities near the nozzle decrease quickly AEFI, producing flames that cannot propagate quickly downstream to consume the main fuel charge. Therefore, ignition at times close to the end of injection is desirable. However, short delays AEFI reach another limit when the mixture is too fuel rich.

Figure 7 illustrates the trade-off between misfire and decreased combustion efficiency. Optimal ignition timings are found between these two regimes. The rapid changes to mixture equivalence ratio and velocity that occur at the end of injection make the window for successful ignition quite narrow. Variance in these processes at the end of injection is also likely to cause higher variance in ignition and flame growth, particularly for ignition systems (such as a laser) that attempt to ignite mixtures in very short time durations. Although these results are shown for a combustion vessel with gases that are quiescent prior to injection, the same principles of operation may be expected in an engine. Spark timings in spray-guided GDI engines are typically AEFI [3]. Accordingly, the flame must be capable of propagating from the spark location to the downstream fuel charge that has already been injected. As mentioned in the Introduction, convection of the kernel downward and away from conventional spark electrodes is critical for propagating flames in actual GDI engines [5]. Low combustion efficiency results when the flame stays near the spark plug and does not propagate into the piston bowl [6].

LASER-INDUCED IGNITION OF MULTI-PULSE FUEL INJECTIONS

Building from the single-injection characterization of laser ignition, we can now address ignition when using multiple injections. The multiple-injection timing is shown on the single-injection ignition regime map in order to understand how the injection timing is interconnected to the ignition timing from single-injection events. Four different laser timings will be shown, all with the same double-injection schedule.

The double-injection schedule, and timing of the laser pulse, are shown at the top of Figure 8 in blue and red lines, respectively. The injector duty cycle is two 400-μs injections, separated by a dwell of approximately 350 μs. This injection schedule attempts to minimize the dwell between injections, to maintain equal injection duration for each injection, and to preserve similar timing for the overall start and end of all injections compared to the single injection (*i.e.*, total duration is approximately 1200 μs). The dwell time of 350 μs is the minimum limit for stable operation of the injector. Minimizing dwell is also desired to allow delivery of enough fuel for a given engine load. Table 1shows that the total fuel delivery is approximately 75% of that using a single, 1200-μs injection.

Akin to previous images, the combustion regime in Figure 8 is shown relative to the end of the first injection. The second injection begins in a time period where laser ignition is successful with only a single injection. The laser timing shown as a vertical red line in Figure 8 is 420 μs AEFI, which is shortly after the start of the second injection.

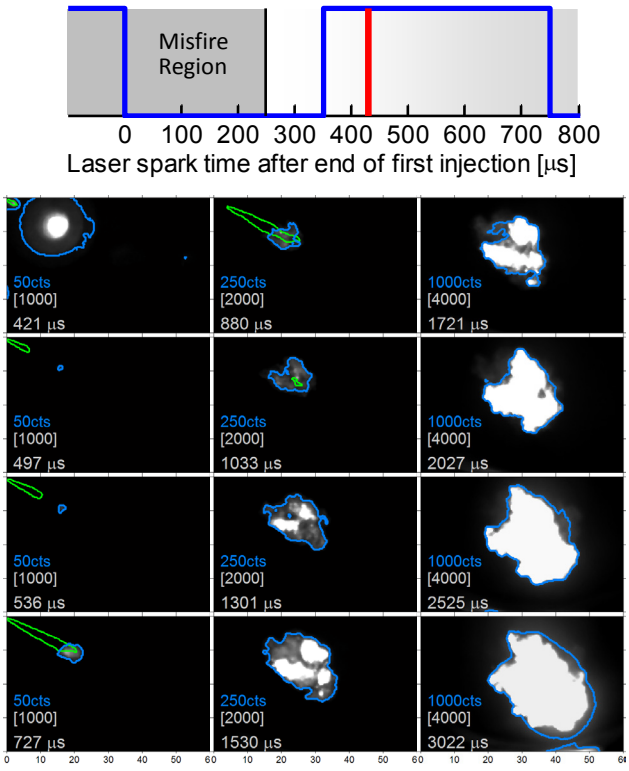

Figure 8: Laser ignition of double injection 420 μs after end of first 400-μs duration injection (timing schematic shown at top with injection schedule in blue and laser timing in red). Image format at the bottom the same as Fig. 5.

Similar to the format followed in the presentation of the single injection data, the bottom of Figure 8 shows a high-speed luminosity image sequence detailing the laser plasma formation, flame kernel development, and flame growth. Note that the images commence with the laser plasma formation; hence, the green line denoting the liquid border of the spray is that of the second injection. The grayscale and threshold boundary count levels are varied as before, but the axial distance of fuel vapor (a white dashed line in Figure 5) is not shown.

At the beginning of the sequence shown in Figure 8, strong plasma emission that illuminates upstream liquid near the injector is apparent. Injection has begun, but the liquid fuel spray has only penetrated a few mm. By 500 μs AEFI, a flame kernel is already distinguishable, similar to the kernel growth shown for the single injection in Figure 5. The second-injection spray penetrates towards the flame kernel and reaches the kernel by 700 μs AEFI. With increasing time AEFI, the spray appears to deform the growing flame zone, splitting it apart into a lower and upper region after the end of injection. In particular, images at 1300 and 1500 μs AEFI show two separate bright regions split by the spray. These bright regions continue to grow and become very intense, completely saturating the camera. The intensity of the luminosity, compared to chemiluminescence levels, suggests that this luminosity is soot incandescence indicative of fuel-rich combustion.

By all measures, the ignition and combustion appear strong and robust for the conditions of Figure 8. The flame kernel grows quickly after the time of laser plasma. The flame also moves downstream rapidly to reach the fuel charge away from the injector. These are characteristics of robust ignition as suggested by the experiments examining laser timing in the single-injection ignition regime. In addition, the convective activity of the second injection also appears to enhance the combustion substantially, including a "pull" of the flame downstream to reach the charge that was already delivered by the first injection. Even though combustion is active prior to the arrival of the second injection, the flame does not propagate upstream to the injector, as previously discussed for the single-injection experiments. Similar results are shown in lifted spray flames where the flame is already activated during injection [25]. The flame does not propagate back towards the injector, leaving a source of unburned fuel near the injector [27]. We will discuss the net effect of the flame movement on overall combustion efficiency in the next section, after exploring the flame growth as a function of laser timing.

Figure 9 shows the effect of delaying the laser timing only 100 μs compared to Figure 8. With the laser pulse arriving at 520 μs AEFI, ignition of single injections is possible, but with reduced combustion efficiency. As expected, the luminosity image sequence shows

that the penetrating spray is now much closer to the focal spot, and the bright plasma emission once again illuminates the liquid fuel. A flame kernel develops prior to arrival of the spray at 600 μs AEFI, but it is quite weak and small compared to that shown for the earlier laser timing. The flame kernel has had less time to develop prior to arrival of the spray from the second injection, and the mixture is more fuel-lean because of the extra delay AEFI. As a result, the flame is barely visible, even displayed at low grayscale counts range.

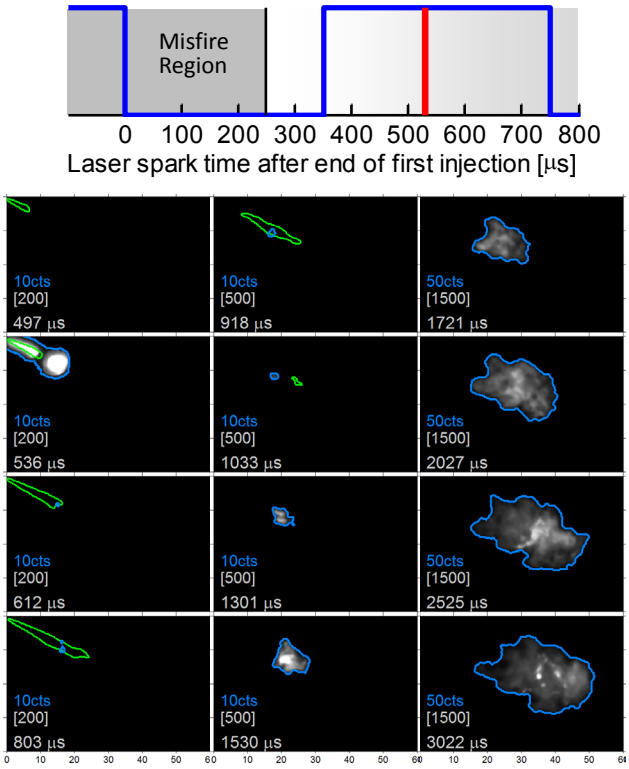

Figure 9: Laser ignition of double injection, 520 μs after end of first 400-μs duration injection (timing schematic shown at top). Image format the same as Fig. 5.

As the spray passes through the growing kernel, the flame once again appears split by the penetrating spray. However, in contrast to a laser timing of 420 μs AEFI, there is no significant growth in the size or intensity of the flame luminosity region from 800 to 1000 μs AEFI. The penetrating spray appears to have a quenching effect on the flame growth, as would be expected for an incoming spray of fuel-rich mixture and high turbulence.

Unlike the single-injection misfire event that decays within 300 μs AEFI (Figure 6), the heat and combustion radicals of the developing flame do persist, surviving a direct hit by the second injection spray, and the flame grows quite rapidly after the spray passes. The flame moves quickly in the convective direction of the spray, and after 2000 μs AEFI the border of the flame is in approximately the same position as that with earlier laser timing (Figure 8). One major difference between the 420-μs and 520-μs laser timings is that the flame luminosity is much lower, concomitant with chemiluminescence, rather than soot incandescence. This indicates that the combustion is mainly non-sooting.

The lack of soot formation, coupled with the fact that the flame area ultimately encompasses the same region as that for the condition with earlier laser timing, which did form soot, suggests that there could be benefits to this particular laser timing regime when coupled with multiple injections. Shortly after the laser plasma timing (within approximately 600 μs), the flame growth did not look promising. The flame was quite weak and growing slowly. Should this have been a single injection, the flame would have had difficulty reaching the downstream fuel charge, consistent with the decreased combustion efficiency shown in Figure 7. However, the second injection acted as a delivery source (like a blow torch) to propel the flame to the downstream fuel charge. Again, we will discuss the net effect of the flame movement on overall combustion efficiency in the next section.

Given that increasing the laser timing AEFI is found to generate a sustained flame with reduced soot formation, we explored further delays in the arrival of the laser pulse. Figure 10 shows the observed combustion event with a laser timing of 730 μs AEFI. In this

case, the second spray has already arrived at the focal spot at the time of laser plasma formation. Similar to the single injection result shown in Figure 6, the flame kernel does not survive and the condition is a complete misfire. The cause of the misfire is definitely the second-injection spray. Ignition attempts with this same timing for a single injection show successful ignition, albeit with lower combustion efficiency according to the combustion regime diagram. Therefore, propagation of the second-injection spray has further limited the allowable laser timings for successful ignition with multiple injections.

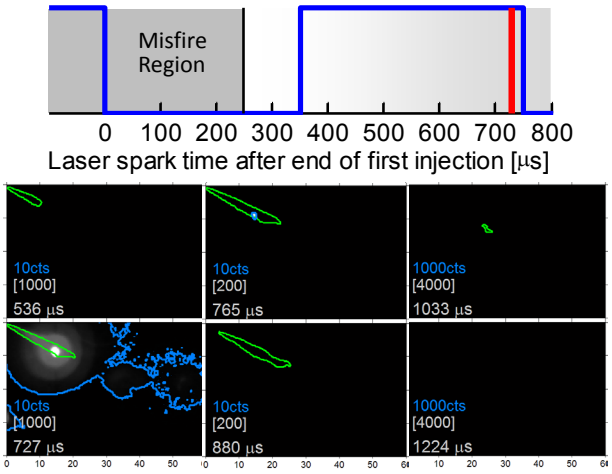

Figure 10: Laser ignition of double injection, 730 µs after end of first 400-µs duration injection (timing schematic shown at top). Image format the same as Fig. 5.

Finally, Figure 11 shows the results when the laser timing is delayed so that the laser pulse arrives after the end of the second injection. The combustion regime at the top now shows two misfire periods, corresponding to each injection. The timing at 1110 µs AEFI falls within the successful ignition regime after the end of the second injection (360 µs AESI).

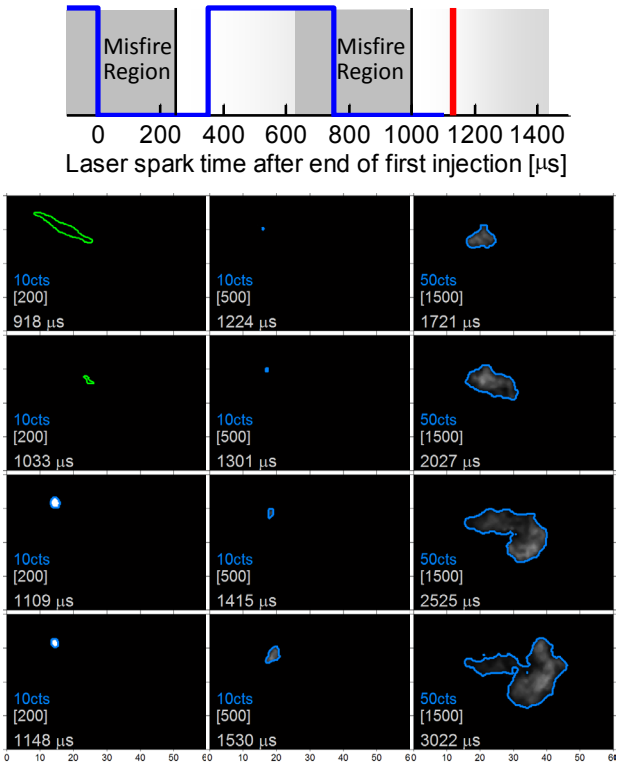

Figure 11: Laser ignition of double injection, 1100 μs after end of first 400-μs duration injection (timing schematic shown at top). Image format the same as Fig. 5.

The luminosity image sequence shows that after the plasma decays the flame kernel remains small for approximately 500 μs. Subsequent flame growth occurs after 1500 μs AEFI, well after the end of both injections. Thus, there has been ample time for the fuel charge to disperse and become more fuel-lean. As a result, the combustion chemiluminescence is less intense, and the flame does not grow as much. For comparison, the images in the far right panel of Figure 11 are shown at the same timings as those presented in Figure 9. Clearly, the flame area is smaller and the luminosity is much less at equivalent times AEFI for the laser delay timing of 1100 μs AEFI. These are indications that the combustion efficiency decreases when using laser ignition after the end of the second injection.

Combustion efficiency

The luminosity imaging described above provides visual information about the flame growth, but it does not give a quantitative assessment of the heat release or combustion efficiency. In this section, we evaluate the combustion efficiency by analyzing the pressure rise in the combustion vessel as a measure of the total energy released from combustion for the laser timings discussed in the previous section. We find that ignition after the end of the double injection produces less energy release than if laser ignition is initiated between the two injections. Pressure rise measurements for the individual double injections given in Figure 8 to Figure 11 are analyzed and shown in Figure 12. Because of the large volume of the combustion vessel, the pressure rise is quite small relative to the absolute pressure, which creates uncertainty in the measured pressure of approximately 1 kPa for these conditions. As such, the pressure measurements given in Figure 12 are low-pass filtered to reduce noise.

As shown in Figure 12, ignition after the end of the double injection (1100 μs AEFI), produces a slower pressure rise with a lower total heat release than ignition timings between injections, indicating lower combustion efficiency. Conversely, the two ignition timings between injections (420 μs and 520 μs AEFI) produce a faster pressure rise and a similarly high total heat release. For example, markers are given at 3020 μs AEFI in Figure 12, which corresponds to the last image time in the luminosity image sequences above. As a reference to engine timescales and the need to complete heat release in a timely fashion, 3020 μs corresponds to 36 crank-angle degrees in an engine operating at 2000 rpm. With a target crank angle of injection of 30° BTDC, 3020 μs AEFI is a time when the piston is already 6° past top-dead center. At 3020 μs AEFI, Figure 12 shows that the pressure rise when igniting after both injections is less than 50% of that when successfully igniting between injections. The rate of pressure rise at any time is also

much lower, again less than 50% of conditions with ignition between injections. Combustion continues after 3020 μs AEFI, and pressure continues to rise for all conditions, but the retarded combustion becomes more difficult to complete, particularly in an engine where the piston would now be rapidly expanding. At 6000 μs AEFI, the pressure rise when igniting after both injections is still low, amounting to about 75% of that when igniting between injections. The failed ignition attempt at 730 μs AEFI, which was quenched by dense, fuel-rich regions of the second injection, produces no pressure rise, as expected.

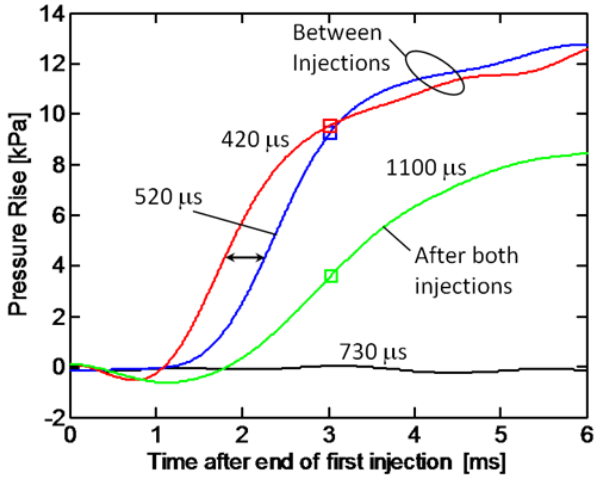

Figure 12: Measured pressure rise after laser ignition of double injections. Times shown adjacent to each curve are laser-ignition time relative to the end of first 400-μs duration injection.

As discussed previously, the key difference observed between these cases lies in the flame kernel convection and propagation down through the stratified charge. With ignition between sprays, when velocities are relatively low and liquid fuel has largely vaporized at the ignition location, the initial kernel can develop far enough along so that the second injection carries the developing kernel down into the charge from the first injection. With ignition after the end of a single or double injection, the conditions at the ignition location can support a developing flame kernel, but it must then propagate on its own through the stratified charge. As seen in Figure 11, the flame propagation for ignition AESI is slower and does not appear to propagate fully through the charge in comparison to cases with ignition between sprays (Figure 8 and Figure 9). Figure 12 confirms the flame propagation trends seen in the high-speed images, showing that there can be a substantial improvement in combustion efficiency for a properly timed ignition event between two injections. This strategy leverages the momentum of the second spray to promote flame propagation through the stratified charge.

Further examination of pressure rise for the two conditions with successful ignition between injections illustrates the high sensitivity in flame propagation dependent upon the ignition timing. While the laser timing is phased by only 100 μs, Figure 12 shows that the major portion of heat release is phased by approximately 500 μs as indicated by the double arrow. The image sequence given in Figure 9 for the 520-μs condition shows that the interaction of the second injection with the early flame kernel is responsible for this delay. The early flame kernel remains small until approximately 1300 μs AEFI, producing heat release or pressure rise that is below experimental resolution. However, the flame eventually grows quickly and the pressure rise meets, and exceeds, the 420-μs condition. Therefore, the delayed heat release does not ultimately impair the completion of combustion for the 420-μs condition.

Combustion luminosity

To extend the analysis beyond imaging, in this section we present the total luminosity measured by a photodiode from the bottom view of the combustion vessel for the laser timings discussed in the previous section. Figure 13 shows that these laser timing are directly measured by the photodiode, appearing as an impulse at their respective timings. Figure 13 shows that the total luminosity depends upon the laser timing, increasing from zero with no combustion (730 μs AEFI) to maximum luminosity at 420 μs AEFI. Though Figure 12 shows a nearly equivalent energy release for ignition timings between injections (420 μs and 520 μs AEFI), Figure 13 reveals that the earlier timing (420 μs AEFI) produces a total integrated combustion luminosity that is more than 60 times greater than that for the ignition timing of just 100 μs later (520 μs AEFI). As discussed previously, this luminosity likely arises from the products of fuel-rich combustion and the incandescence of hot soot. Thus, there appears to be a narrow optimal ignition timing window between sprays that produces robust, soot-free combustion.

The luminosity levels also depend upon laser timing when the luminosity is dominated only by chemiluminescence. For example, the total integrated luminosity levels recorded from the ignition event at 520 μs show luminosity levels is higher than the luminosity emitted from late ignition AESI (1100 μs AEFI). This difference is corroborated by the high-speed imaging discussed above. Chemiluminescence appears weak when igniting after the second injection, which is representative of mixtures that are more fuel-lean and burning at lower flame temperature. The volume of the flame is also smaller when igniting after the second injection. These observations also consistent with a reduction in combustion efficiency, as discussed in the previous section.

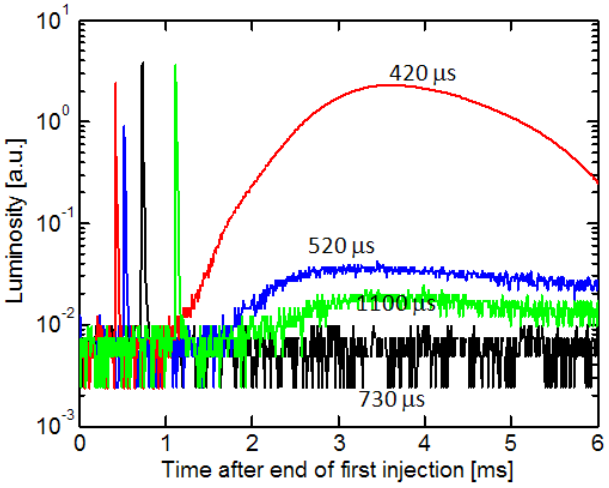

Figure 13: Measured luminosity from bottom-view photodiode after laser ignition of double injections. Times shown adjacent to each curve are laser-ignition time relative to the end of first 400-μs duration injection.

To summarize these results, Figure 14 shows a schematic of the different combustion regimes observed for the laser ignition of two 400-μs fuel injections. As for a single injection, laser timings until approximately 250 μs AEFI result in misfire and ignition is not successful. A second misfire region occurs when the spray from the second injection overlaps the ignition location between approximately 620 μs and 1000 μs AEFI. In both of these regions, the plasma immediately extinguishes and no flame kernel is formed. Misfire results because these mixtures are likely too fuel-rich to support flames, coupled with the fact that there are high scalar and velocity gradients and a high density of liquid droplets, both of which are unfavorable to flame growth. When the laser timing is delayed until after the end of the second injection, ignition is possible, but akin to single-injection operation, decreasing combustion efficiency is observed with increasing time AESI. At these ignition timings, mixtures at the ignition location mix rapidly and become increasingly fuel-lean with time. As a result, the flame displays lower combustion chemiluminescence and a low total heat release. In addition, flame speeds become slow in these mixtures and the flame does not propagate fully through the stratified charge.

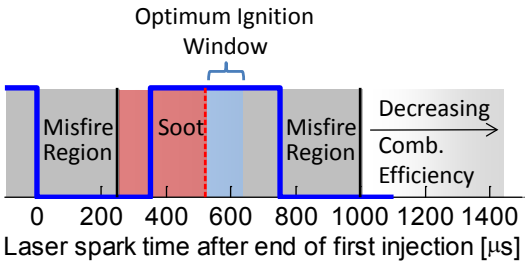

Figure 14: Schematic of successful ignition window for laser-induced ignition of a double fuel injection.

Laser timings between the two 400-μs fuel injections produce successful ignition and the highest combustion efficiencies. However, the resulting combustion regime within that window is very sensitive to small variations in laser timing. Laser timings that occur too early after the end of the first injection (after 250 μs and up to 520 μs AEFI) have a longer time for a strong kernel to develop prior to the arrival of the second injection. As a result, the second injection is rapidly ignited and the charge burns in a fuel-rich combustion regime that produces soot. The main benefit of forming a flame kernel between in injections lies in coupling the growing flame kernel with convection produced by the second injection. The second injection helps to transport the flame down into the charge remaining

from the first injection, completing combustion through the stratified charge. Thus, if the laser timing is delayed just long enough in this window to ensure adequate kernel development prior to the arrival of the second injection, the kernel can survive a direct hit by the spray and benefit from this convective transport, while delaying flame propagation through the fuel-rich second injection. The schematic in Figure 14 shows that there is a narrow window of potential laser-ignition timings from 520 μs AEFI until reaching the misfire region at 620 μs AEFI where this injection-assisted flame propagation occurs without evidence of soot. Due to the narrow time period of this optimal ignition window (about 100 μs), this regime would not be accessible by conventional electric spark ignition with spark durations on the order of 1-2 ms. The precision ignition timing and short spark duration obtained by laser ignition may offer advantages for combustion efficiency and emissions control in spray-guided SIDI engines.

SUMMARY/CONCLUSIONS

The use of laser-induced spark ignition has been investigated in single and dual-injection sprays from a multi-hole nozzle GDI injector. One of the benefits of laser spark ignition is that laser sparks offer precision timing capabilities that are not possible with current conventional electric spark systems. Thus, we exploited this unique characteristic to study the influence of ignition timing on the kernel development, flame propagation and combustion of stratified charges.

High-speed luminosity imaging of ignition and flame propagation, along with pressure rise and integrated luminosity measurements revealed that for the ignition of single injection sprays:

- Laser timings during the injection event do not result in successful ignition.
- Laser timing after the end of injection, when the ignition location is largely free of liquid droplets and mixtures are more fuel-lean, result in successful ignition.
- Due to rapid mixing after the end-of-injection, combustion efficiency decreases as the laser timing occurs later after the end of injection.

For the ignition of dual 400-ms injections:

- As for single injections, laser timing during either of the two injection events results in misfire.
- As for single injections, laser timing after the end of both injections results in successful ignition, but with decreasing combustion efficiency as the laser timing is further retarded AESI.
- Laser ignition between sprays results in high combustion efficiency, where flame propagation is assisted by the convective interaction between the developing kernel and the second injection.
- The time window for leveraging this injection-assisted flame propagation is relatively narrow, limited on either side by the presence of the first or second spray in the ignition location.
- This time window is further narrowed by timings that result in fuel-rich sooting combustion, where the initial kernel development progresses too far before the arrival of the second injection, quickly igniting the newly arrived fuel-rich mixture.
- An optimal ignition timing window of just 100-μs exists for this operating condition, where injection-assisted flame propagation is observed along with soot-free combustion.
- Accomplishment of this timing requires ignition timing control on the order of 0.1 ms, which is much shorter than current electric spark ignition systems that have spark duration on the order of 1.0 ms. Therefore, the benefits of this ignition strategy are only realized with the use of a short-pulse laser ignition system.

REFERENCES

1. Kneifel, A., Buri, S., Velji, A., Spicher, U., Paper, J. and Sens, M., “Investigations on Supercharging Stratified Part Load in a Spray-Guided DI SI Engine,” SAE Paper 2008-01-0143.
2. Piock, W.F., Weyand, P., Wolf, E. and Heise, V., “Ignition Systems for Spray-Guided Stratified Combustion,” SAE Paper 2010-01-0598.
3. Drake, M.C., Fansler, T.D., and Lippert, A.M., "Stratified-charge combustion: modeling and imaging of a spray-guided direct-injection spark-ignition engine," *Proceedings of the Combustion Institute* **30**:2683-2691, 2005.
4. Dahms, R., Fansler, T.D., Drake, M.C., Kuo, T.W., Lippert, A.M., and Peters, N., "Modeling ignition phenomena in spray-guided spark-ignited engines," *Proceedings of the Combustion Institute* **32**:2743-2750, 2009
5. Fansler, T.D., Drake, M.C., and Böhm, B., "High-Speed Mie-Scattering Diagnostics for Spray-Guided Gasoline Engine Development," Proceedings of the 8th International Symposium on Internal Combustion Engine Diagnostics, Baden-Baden, June 2008.

6. Peterson, B., Reuss, D.L., and Sick, V., "High-Speed Imaging Analysis of Misfires in a Spray-Guided Direct Injection Engine," *Proceedings of the Combustion Institute*, doi:10.1016/j.proci.2010.07.079, 2010.
7. Hese, M., Tschoke, H., Breuninger, T., Altenschmidt, F. and Winter, H., "Influence of a Multispark Ignition System on the Imflammation in a Spray-Guided Combustion Process," SAE Paper 2009-24-0117.
8. Febler, M., Wetzel, M., Schenk, M., Rottengruber, H., and Huhn, W., "Determination of Thermodynamic Potentials for Alternative Ignition Systems in Spray-Guided Combustion," Proceedings of the 8th International Symposium on Internal Combustion Engine Diagnostics, Baden-Baden, June 2008.
9. Orlandini, I., Gartung, K. and Schlerfer, J., "Application of 3D-CFD Simulations in the Development of Spark Plugs," SAE Paper 2009-01-0706.
10. Husted, H.L., Plock, W. and Ramsay, G., "Fuel Efficiency Improvements from Lean, Stratified Combustion with a Solenoid Injector," SAE Paper 2009-01-1485.
11. Schwarz, Ch., Schunemann, E., Durst, B., Fischer, J. and Witt, A., "Potentials of the Spray-Guided BMW DI Combustion System," SAE Paper 2006-01-1265.
12. Yun, H., Wermuth, N. and Najt, P., "Development of Robust Gasoline HCCI Idle Operation Using Multiple Injection and Multiple Ignition (MIMI) Strategy," SAE Paper 2009-01-0499.
13. Bradley, D., Sheppard, C.G.W., Suardjaja, I.M. and Woolley, R., "Fundamentals of High-Energy Spark Ignition with Lasers," Combustion and Flame **138**: 33-77, 2004.
14. Groß, V., Kubach, H., Spicher, U., Schießl, R., and Maas, U., "Influence of Laser-Induced Ignition on Spray-Guided Combustion – Experimental Results and Numerical Simulation of Ignition Processes," SAE Paper 2009-01-2623, 2009.
15. Phuoc, T.X., "Laser-induced spark for simultaneous ignition and fuel-to-air ratio measurements," *Optics and Lasers in Engineering* **44**:520-534, 2006.
16. Tsunekane, M., Taira, T., Inohara, T., and Kanehara, K., "Efficient ignition of a real automobile engine by a high brightness, passively Q-switched Cr:YAG/Nd:YAG micro-laser," 2010.
17. Engine Combustion Network data archive. <http://www.sandia.gov/ECN/> .
18. Pickett, L.M., Genzale, C.L., Bruneaux, G., Malbec, L.-M., Hermant, L., Christiansen, C.A., and Schramm, J., "Comparison of diesel spray combustion in different high-temperature, high-pressure facilities," SAE Paper 2010-01-2106, 2010.
19. Pickett, L.M., Kook, S., and Williams, T.C., "Visualization of Diesel Spray Penetration, Cool-Flame, Ignition, High-Temperature Combustion, and Soot Formation Using High-Speed Imaging," *SAE Int. J. Engines* 2:439-459, 2009 (Paper 2009-01-0658).
20. Siebers, D.L., "Liquid-Phase Fuel Penetration in Diesel Sprays," SAE Paper 980809, 1998.
21. Settles, G.S., *Schlieren and Shadowgraph Techniques*, Springer-Verlag, 2001.
22. Musculus, M.P.B., Lachaux, T., Pickett, L.M., and Idicheria, C.A., "End-of-injection over-mixing and unburned hydrocarbon emissions in low-temperature-combustion diesel engines," SAE Trans. 116(3):515-541, 2007, (Paper 2007-01-0907).
23. Kook, S., Pickett, L.M., Musculus, M.P.B., and Gehmlich, R. K., "Influence of Diesel Injection Parameters on End-of-Injection Liquid Length Recession," *SAE Int. J. Engines* 2:1194-1210, 2009, (Paper 2009-01-1356).
24. Steen, W.M., "Laser Material Processing," Springer-Verlag, London, 2003.
25. Genzale, C. L., Reitz, R. D. and Musculus, M. P. B., "Effects of Piston Bowl Geometry on Mixture Development and Late-Injection Low-Temperature Combustion in a Heavy-Duty Diesel Engine," SAE Paper 2008-01-1330.
26. Pickett, L.M., Kook, S., Persson, H., and Andersson, O., "Diesel fuel jet lift-off stabilization in the presence of laser-induced plasma ignition," *Proceedings of the Combustion Institute* **32**:2793-2800, 2009.
27. Lachaux, T. and Musculus, M.P.B., "In-cylinder Unburned Hydrocarbon Visualization During Low-Temperature Compression-Ignition Engine Combustion Using Formaldehyde PLIF," *Proceedings of the Combustion Institute* **31**:2921-2929, 2007.

CONTACT INFORMATION

Caroline L. Genzale, clgenzale@gmail.com

Lyle M. Pickett, LMPicke@sandia.gov

ACKNOWLEDGMENTS

Support for this research was provided by the U.S. Department of Energy, Office of Vehicle Technologies. The research was performed at the Combustion Research Facility, Livermore, California. Sandia is a multiprogram laboratory operated by Sandia Corporation, a Lockheed Martin Company, for the United States Department of Energy's National Nuclear Security Administration under contract DE-AC04-94AL85000.

DEFINITIONS/ABBREVIATIONS

AEI	After end of injection
AEFI	After end of first injection
AESI	After end of second injection
ATDC	After top-dead-center
BTDC	Before top-dead-center
CAD	Crank-angle degrees
COV	Coefficient of variation
EOI	End of injection
GDI	Gasoline direct-injection
IMEP	Indicated mean effective pressure
Nd:YAG	Neodymium-doped Yttrium Aluminum Garnet
SIDI	Spark-ignition direct-injection
SOI	Start of injection